Molecular Modeling Studies on Zeolite Catalysts for Shape-Selective Electrophilic Substitution: I Acylation of 2-Methoxynaphthalene

Patibandla Bharathi, Suresh B. Waghmode, Subramanian Sivasanker, and Rajappan Vetrivel*

Catalysis Division, National Chemical Laboratory, Pune-411008, India

(Received February 17, 1999)

The diffusion characteristics of acylated 2-methoxynaphthalene inside large pore zeolites were investigated. The interaction of the three isomers with fully siliceous zeolite lattices was studied by energy-minimization calculations. The favorable adsorption sites and the orientation of the acylated products of 2-methoxynaphthalene were analyzed in detail. Three large pore zeolites having 12 m channels were selected: (i) mordenite with an elliptical 1-d channel, (ii) zeolite-L with a circular channel and 2-d cages, and (iii) zeolite-β with circular 3-d channel systems. It was observed that the shape selectivity properties of the zeolites could be profitably used to produce 2-acyl-6-methoxynaphthalene. In the case of mordenite, the diffusion of all three isomers is facile, whereas in the case of zeolite-L, the diffusion of 1-acyl-7-methoxynaphthalene is more facile than 2-acyl-6-methoxynaphthalene and 1-acyl-2-methoxynaphthalene. In the case of zeolite-β, the energy barrier for the diffusion of 2-acyl-6-methoxynaphthalene is significantly smaller than those of the other two isomers. Thus zeolite-β is predicted to be a suitable catalyst for the shape-selective acylation of 2-methoxynaphthalene to 2-acyl-6-methoxynaphthalene.

2-Acyl-6-methoxynaphthalene is the key intermediate for the production of (*S*) -2-(6-methoxy-2-naphthyl)propanoic acid, a popular non-steroidal anti-inflammatory drug with the international non-proprietary name naproxen.[1—3] Additionally, naproxen has been claimed to be a useful additive in skin care and skin damage control compositions.[4,5] Aryl ketones, are generally intermediates for various pharmaceutical products and fragrant molecules.[6] The Friedel Crafts acylation of aromatics has generated continuous and sustained interest.[7] Conventionally, acyl chlorides together with a stoichiometric amount of a Lewis acid, (e.g. $AlCl_3$, $FeCl_3$ or $TiCl_4$) are used for this reaction.[8,9] The synthetic utility of this reaction is limited by the formation of a considerable amount of byproducts and toxic wastes. The use of Bronsted acid catalysts, such as polyphosphoric acid,[10] promotes side reactions, such as cyclization, aromatization and dehydration.

Alternatively, solid acid catalysts are useful in the acylation of aromatics and the specific catalysts attempted for acylation of 2-methoxynaphthalene (**1**) include La–Ce–Y,[11] zeolite-β,[12] several other zeolites,[13—16] MCM-41,[17] cation exchanged clays,[18] alumina pillared clays,[19] etc. Although the acylation of **1** leads to a kinetically controlled products, namely 1-acyl-2-methoxynaphthalene (**2**), 2-acyl-6-methoxynaphthalene (**3**), can be selectively produced by the acylation of **1** by controlling the reaction conditions.[20] Minor amounts of 1-acyl-7-methoxynaphthalene (**4**) are also known to be formed.[18] In the acylation of **1**, the interplay between the electronic and steric factors control the selectivity. As mentioned earlier, it is possible to alter the selectivity by varying the reaction conditions[21,22] and the steric factor could be favorably utilized to achieve the selectivity for **3**. In this work, we applied molecular modeling techniques in order to study the diffusion characteristics of molecules **1** to **4** in the 12 member (12m) channels of mordenite (MOR), zeolite-L (LTL), and zeolite-β (BEA). The diffusivity of the molecules and the shape-selective efficiency of the three zeolites with different dimensionality were investigated by analyzing the results of energy-minimization calculations.

Methods and Models

The computational studies reported here were carried out using software programs supplied by Molecular Simulations Inc., USA. The force-field energy-minimization calculations were performed with the discover program, using a consistent valence force field (CVFF) of Hagler et al,[23] and the parameters were obtained from the reports of Dauber–Osguthorpe et al.[24] The actual values used are listed in our earlier paper.[25] The interaction energy of the molecule with the zeolite framework was calculated using a force-field expression containing terms corresponding to the deformation of the bond lengths, bond angles, torsion angles, etc. The non-bonding interactions of the molecule with a zeolite framework were calculated by determining the long- and short-range forces in terms of the electrostatic interaction and Lennard–Jones potentials. Molecular graphics displays were obtained from the Insight II molecular modeling system using a SiliconGraphics workstation. Energy-minimization was carried out in a sequence with steepest-descent, conjugate gradient and Newton–Raphson algorithms.

The extents of the molecule in space were calculated for an energetically favorable conformation and their sizes and shapes were analyzed. The dimensions of the molecules in three-dimensional

space were measured according to a procedure detailed elsewhere.[26] The three largest dimensions of the molecules ($a \times b \times c$) in mutually perpendicular directions are given in Table 1. The qualitative structural fitting of the molecules inside the zeolites was studied by molecular graphics (MG) as well as by comparing the dimensions of the molecules with the pore diameters of the zeolites, given in Table 2. It was observed that the small-pore and medium-pore zeolites are too small to fit these molecules. Three large-pore zeolite lattices were generated from the X-ray crystal structures reported for MOR,[27] LTL,[28] and BEA.[29] Further, the chemical interaction between the zeolite host–guest molecules was studied using energy-minimization calculations in order to understand the adsorption sites and diffusion characteristics of molecules **1** to **4** shown in Fig. 1. The simulation box contained the generated zeolite, based on its crystal structures; the actual dimensions of the simulation box for each zeolite are given in Table 2. The sizes of the simulation boxes were chosen in such a way that the symmetry along the channel direction was taken care of and the box was just large enough in the other two directions to take care of the non-bonded interactions.

Table 1. Dimensions of 2-Methoxynapthalene and Its Three Possible Acylated Products in Their Minimum Energy Configuration

Molecule (Numbering as in Fig. 1)	Dimensions		
	a / Å	*b* / Å	*c* / Å
1	10.0	6.0	2.8
2	10.3	8.1	4.1
3	12.3	6.2	2.8
4	10.5	7.8	2.8

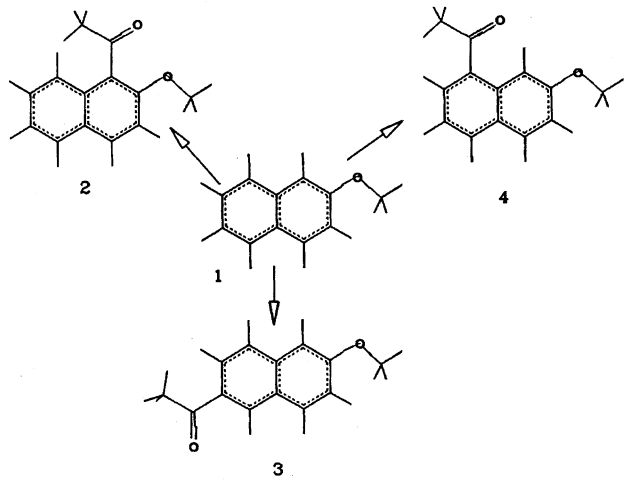

Fig. 1. 3d molecular graphics pictures of 2-methoxynaphthalene (**1**) and its possible acylated products: 1-acyl-2-methoxynaphthalene (**2**), 2-acyl-6-methoxynaphthalene (**3**), and 1-acyl-7-methoxynaphthalene (**4**).

The calculations were performed following the well-estabilished forced-diffusion procedure. This procedure was developed and described by Horsley et al.[30] in an investigation of the shape-selectivity properties of zeolites in the alkylation of naphthalene. Several manifestations of this procedure have been successfully used in many studies to predict the diffusion characteristics of molecules inside zeolites.[31—35] In the present study, the sorbate molecule was forced to diffuse in regular steps of 0.2 Å along a diffusion path defined by the initial and final positions within the channel. C_2 of the napthalene ring was taken as reference atom. At each point, a strong harmonic potential constrains the molecule to lie at a fixed distance from the initial position, while the energetically favorable conformation and orientation are derived by varying their internal degrees of freedom of the molecule as well as non-bonding interaction of the molecules with the zeolite framework.

During these calculations of the interaction energy, the atoms in the zeolite lattice are held fixed at their crystallographically determined geometries, whereas the molecules are flexible. Since our interest was to study the influence of the pore architecture and dimensions on the diffusion characteristics of the molecules, we considered a fully siliceous zeolite lattice. Thus, the diffusion-energy profile is a graph showing the variation in the interaction energy between the molecule and the zeolite framework as the molecule diffuses within the channel of the zeolite. These profiles are useful to identify the most favorable (minimum energy) and unfavorable (maximum energy) adsorption sites for the molecules inside the zeolite channels. The difference in energy between the most favorable and most unfavorable sites in the diffusion energy profile gives the diffusion energy barrier for the self diffusivity. The influence of the presence of more molecules on the diffusivity (mutual effect) is not considered here. The mean energy is the numerical average of the interaction energy of the molecules at all locations. The ratio of the mean energy/minimum energy is a parameter which indicates the diffusivity of the molecule. If the mean energy is close to the minimum energy, the situation represents the presence of several minima, and the mean/minimum energy ratio will be closer to 1. On the contrary, if the mean energy is far from the minimum energy, the situation represents the presence of several maxima. Thus, the ratio is an indicator of the diffusivity of the molecule.

Results and Discussion

The shape selectivity achieved by zeolites in catalytic conversion is governed by several factors, among which the relative rates of diffusion of the reactants, products and intermediates play a dominant role. Information about the interactions at the molecular level are difficult to derive experimentally. However, the diffusion-energy profiles calculated from the interaction energies predict the interactions at the molecular level, which are useful to derive the diffusion energy barriers, which in turn provide a good indication of the relative rates of diffusion through the pores of the zeolite.

Table 2. Crystal Characteristics and Dimensions of Simulation Boxes for Different Zeolites

Zeolite	Symmetry	Unit cell composition	*a* / Å	*b* / Å	*c* / Å	Average pore diameter (Å)	Number of unit cells in the box
LTL	Hexagonal	$[SiO_2]_{36}$	18.465	18.465	7.476	7.1	$2 \times 2 \times 8$
MOR	Hexagonal	$[SiO_2]_{48}$	18.094	20.516	7.524	7.0×6.5	$2 \times 2 \times 8$
BEA	Tetragonal	$[SiO_2]_{64}$	12.660	12.660	26.406	7.6×6.4	$6 \times 1.6 \times 1$

In the acylation of **1** there is a possibility for the formation of 3 isomers, namely **2**, **3**, and **4**, as shown in Fig. 1.

Structural Fitting: It is a necessary condition that the reactant and the product molecules involved in acylation should fit inside the pores. A comparison of the dimensions of molecules given in Table 1, with those of the pore dimensions of 8m and 10m pore zeolites (pore diameter = ca. 4.0 and 5.5 Å respectively), reveals that the pores of both small- and medium-pore zeolites are too small to accommodate 2-methoxynaphthalene and its acylated products (**2**, **3**, and **4**). We therefore, chose 3 large pore (12m) zeolites with different pore topologies for our studies.

In a molecular-graphics study of large pore zeolites, MOR appeared to be selective, because the shape of the pore matched the shape of isomer **3** better than the shape of isomers **2** and **4**. Isomer **3** has a compact cross-section because the methoxy group, and the acetyl group are in meta positions, as shown in Fig. 1, whereas these components in **2** and **4** are in the ortho position, as shown in Fig. 1. The pores in LTL are circular rather than elliptical with a pore diameter of 7.1 Å. Due to the presence of barrel-shaped cages with 12.6 Å diameter, there may be plenty of room for all of the isomers, there should not be a significant energy barrier for any isomers. However, due to the specific pore architecture, there is a possibility that these cages may help in the formation of isomer **3** selectively. The pores in BEA are elliptical with a pore diameter of 7.6×6.4 Å. The shape of the pore matches the shape of isomer **3** better than that of isomer **2**. BEA appears to be more selective for the formation of isomer **3**. A structural fitting based on MG leads to qualitative results. Further quantitative results can be obtained by incorporating the interaction between the atoms in molecules and zeolite lattice.

Diffusion Energy-Profile Calculation: The calculated diffusion-energy profile symmetrically repeats itself in each unit cell, indicating the validity of our simulation box size, potential parameters and energy minimization calculations. The results of energy minimization calculations for the three zeolites are discussed in the following section.

Diffusion Characteristics of the Molecules in MOR: MOR belongs to an orthorhombic symmetry and has a pore structure that is uni-dimensional. Elliptical 12m channels (7.0×6.5 Å) run along the *c*-direction and the adjacent 12m channels are linked by tortuous 8m channels. Although the 8m channel is too small for the diffusion of the molecules, the side chains of aromatic molecules can be accommodated in the side pockets formed by them. The diffusion of molecules **1**—**4** in MOR was studied for 4 unit cells in the *c*-direction, although the results for product molecules are presented for 2 unit cells in the Figs. 2, 3, and 4. Figure 2 shows a molecular-graphics picture of the minimum-energy configuration of **2** inside MOR. The variation in the interaction energy between **2** and MOR is also included in the form of a graph. Figures 3 and 4 provide similar information for molecules **3** and **4**, respectively. The salient information derived from these diffusion studies are summarized in Table 3. All of the molecules have two minima and two maxima when they

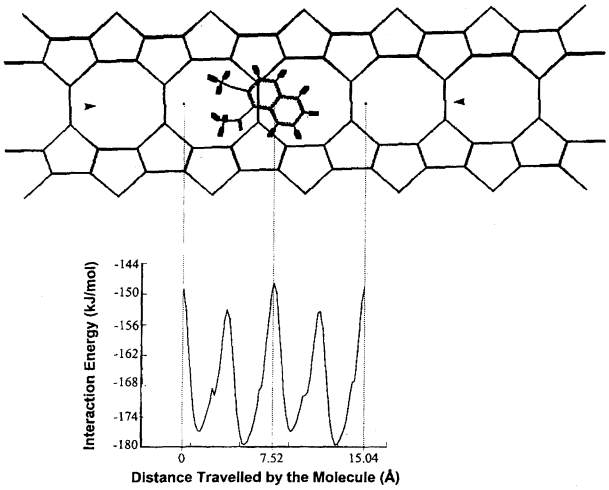

Fig. 2. Variation of interaction energy between **2** and the MOR framework as the molecule diffuses through the 12m channel. The cross section of 12m channel in the '*ac*' plane as viewed through 8m windows is shown. A typical minimum energy configuration of the molecule during the diffusion is also included.

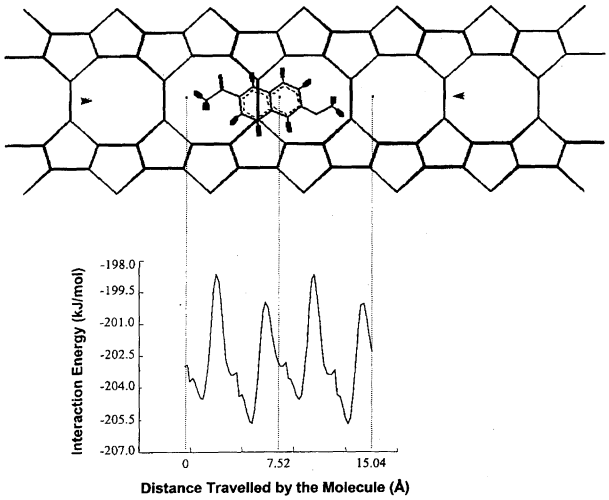

Fig. 3. Variation of interaction energy between **3** and the MOR framework as the molecule diffuses through the 12m channel. The cross section of 12m channel in the '*ac*' plane as viewed through 8m windows is shown. A typical minimum energy configuration of the molecule during the diffusion is also included.

diffuse through one unit cell of MOR, as can be seen in Figs. 2, 3, and 4, although the peak positions are different. The high symmetry along the 12m channel of MOR, compared to the 12m channel of BEA, is also a cause for this observation. Molecules **2** and **4** have a diffusion energy of ca. 30 kJ mol^{-1}; the diffusion energy barrier for **3** is considerably smaller. All of the molecules were found to diffuse with their longest distance along the channel axis. Hence, during the diffusion, the phenyl rings of the molecule are parallel to the 8m rings, as can be seen in Figs. 2, 3, and 4. The mean energy values are also included in Table 3. The diffusivity of the molecule inside the channel is assessed from the ratio of the mean/minimum energy value. For different

Table 3. Salient Energy Parameters Calculated from the Diffusion Energy Profile. Diffusion Energy Barrier (kJ mol^{-1}) and Diffusivity for Reactant and Various Isomers of the Products in Different Zeolites, Which Are Used to Derive Shape Selectivity

Zeolite	Molecule	Energy at peak maximum	Energy at deep minimum (min)	Energy barrier	Mean energy (Mean)	Mean/Min (Diffusivity)
MOR	**1**	−163.476	−170.536	7.060	−166.878	0.979
	2	−148.223	−179.197	30.974	−165.950	0.926
	3	−200.080	−204.498	4.418	−202.291	0.989
	4	−140.076	−170.753	30.677	−144.797	0.848
LTL	**1**	−99.977	−148.821	48.844	−113.453	0.762
	2	−41.757	−166.218	124.461	−130.821	0.787
	3	−71.913	−143.817	71.904	−122.952	0.849
	4	−120.289	−185.860	64.571	−142.592	0.767
BEA	**1**	−147.654	−157.055	9.401	−151.554	0.965
	2	97.603	−177.579	275.182	−135.269	0.762
	3	−178.122	−194.658	16.536	−189.045	0.971
	4	156.286	−163.931	320.217	−130.600	0.797

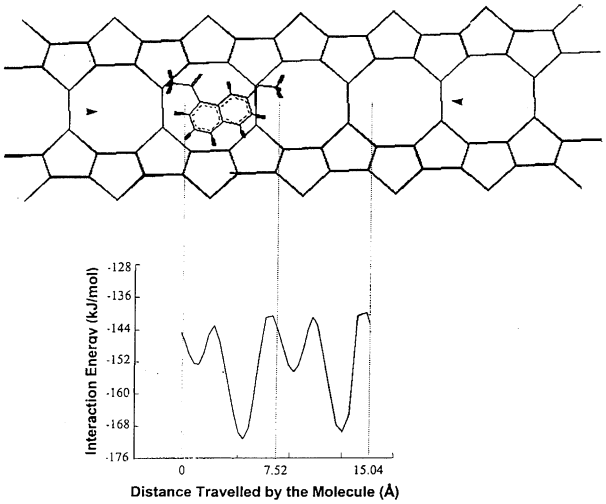

Fig. 4. Variation of interaction energy between **4** and the MOR framework as the molecule diffuses through the 12m channel. The cross section of 12m channel in the '*ac*' plane as viewed through 8m windows is shown. A typical minimum energy configuration of the molecule during the diffusion is also included.

molecules, this ratio decreases in the order **3** > **1** > **2** > **4** inside MOR. This follows the same order predicted by the diffusion energy-barrier values. In addition to the bulkiness of the molecules, a favorable interaction of the side chains in the molecule with the zeolite walls also controls their diffusion behavior.

Diffusion Characteristics of the Molecules in LTL: LTL belongs to the hexagonal crystal class. The pore in LTL is circular with a diameter of 7.1 Å. It has a structure consisting of channels along the *c*-direction. The channels are built up of barrel-shaped 12m rings separated by 7.5 Å along the *c*-direction. The diameter of the barrel is the largest (12.6 Å) at the mid point between the two 12m rings. The diffusion of the molecules along the *c*-direction in the 12m channel is considered. The diffusion calculations were carried out for the reactant and the three possible product molecules. The diffusion was studied for 4 unit cells in the c-direction; the results of such calculations are given in Table 3.

Figure 5 shows a molecular-graphics picture of the minimum-energy configuration of **2** inside LTL. The variation in the interaction energy between **2** and LTL is also included in the form of a graph. Figures 6 and 7 provide similar information for the molecules **3** and **4**, respectively. The salient information derived from these diffusion studies are

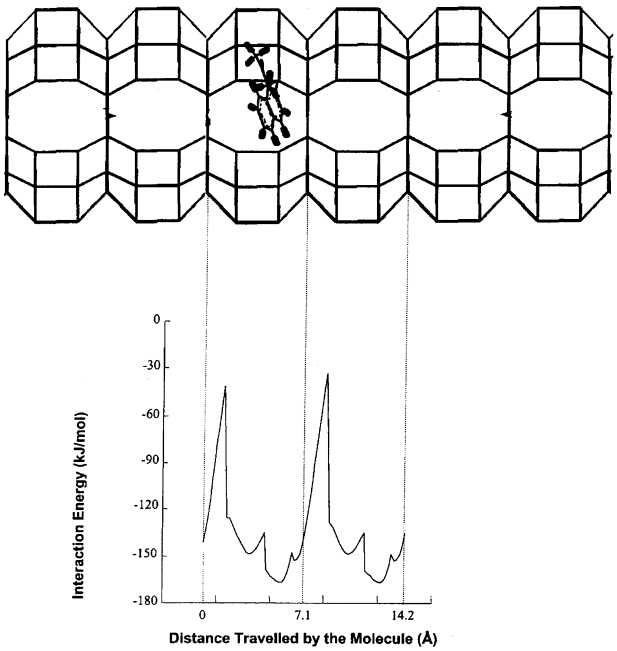

Fig. 5. Variation of interaction energy of **2** and the LTL framework as the molecule diffuses through the 12m channel. The cross section of 12m channel in the '*ac*' plane as viewed through the 8m windows of the barrel-shaped cage is shown. A typical minimum energy configuration of the molecule during the diffusion is also included.

summarized in Table 3. All of the molecules show a single maximum when they diffuse through one unit cell of LTL; since there are barrel-shaped cages, there are several minimum-energy locations for the molecules within a unit cell. Since the empty space in LTL is more than that in MOR, the adsorption energy of the molecules generally less favorable than that in MOR. The energy barriers for the molecules are also much higher in the case of LTL. The diffusivity of the molecules is also less than that in MOR, indicating a longer residence time for these molecules inside LTL. All of the molecules have more tumbling motions inside the barrel-shaped cages of LTL during the diffusion. As they diffuse along, the molecules are more relaxed, and hence the energy at the peak maximum is slightly less along with the progress of diffusion, as typically seen in Fig. 6. In Fig. 7, the pattern of the diffusion energy profile repeats itself after every two unit cells. The dimensions of molecule **4** is almost the same as that of molecule **2**, but is more dynamic due to the non-adjacent positions of the methoxy and acetyl groups in naphthalene. The barrel-shaped cage in LTL provides enough space for **4** to take a perpendicular orientation at the center of the cage. Hence, when it crosses from one cage to another through a 12m ring, there are two possibilities for the molecule to come back to the parallel position. Hence, the energy profile is repeating after two unit cells rather than in every unit cell. The means of the interaction energy values are also included in Table 3. The diffusivity of the molecule inside the channel is assessed by this mean value in relation to the minimum-energy value. The diffusivity of the molecules inside the LTL channel decreases in the order **3** > **2** > **4** > **1**. Thus, when the molecules are much smaller than the cage dimensions, the diffusivity is not related to the size of the molecules. However, the energy barrier of the molecules more or less follows the bulkiness of these molecules. These results indicate the absence of a shape-selective behavior due to diffusion in the case of LTL.

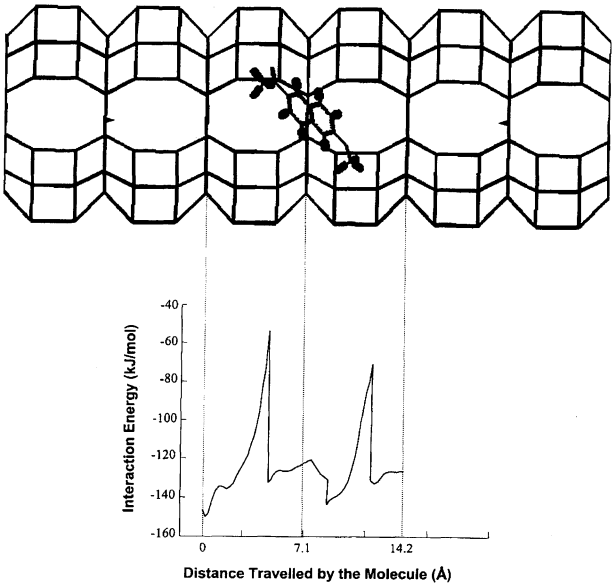

Fig. 6. Variation of interaction energy of **3** and the LTL framework as the molecule diffuses through the 12m channel. The cross section of 12m channel in the '*ac*' plane as viewed through the 8m windows of the barrel-shaped cage is shown. A typical minimum energy configuration of the molecule during the diffusion is also included.

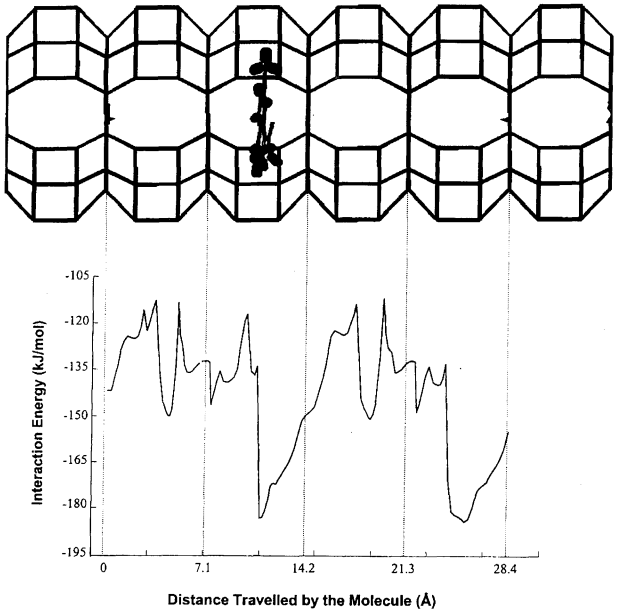

Fig. 7. Variation of interaction energy of **4** and the LTL framework as the molecule diffuses through the 12m channel. The cross section of 12m channel in the '*ac*' plane as viewed through the 8m windows of the barrel-shaped cage is shown. A typical minimum energy configuration of the molecule during the diffusion is also included. The energy variations is shown for 4 unit cells in this case alone, since the pattern repeats after 2 unit cells.

Diffusion Characteristics of the Molecules in BEA: We next chose a three-dimensional zeolite, BEA. BEA has a three-dimensional interconnected channel system with 12m elliptical channels having a diameter of 7.6×6.4 Å. BEA is of great potential industrial interest because of its high acidity and interesting pore architecture. The structure of BEA can be represented as an inter-growth of two well-defined polymorph structures, both of them having a 3d pore architecture. The diffusion of the reactant and the possible three product molecules for the title reaction was carried out along the *a*-direction in the 12m channel. The diffusion was studied for 4 unit cells, although the results are presented for 2 unit cells in Figs. 8, 9, and 10. Figure 8 shows a molecular-graphics picture of the minimum-energy configuration of **2** inside BEA. The variation in the interaction energy between **2** and BEA is also included in the form of a graph. Figures 9 and 10 provide similar information for molecules **3** and **4**, respectively. The salient information derived from these diffusion studies are summarized in Table 3. All of the molecules have one sharp maxima when they diffuse through one unit cell of BEA; this sharp maxima occurs when the molecule moves from one 12m intersection to the other 12m intersection. The adsorption energy of the molecules in BEA is closer to MOR, and the mean-energy values are also closer to the minimum-

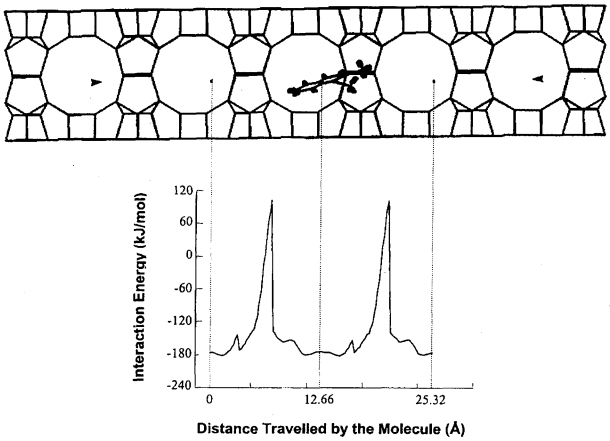

Fig. 8. Variation of interaction energy of **2** and the BEA framework as the molecule diffuses through the 12m channel. The cross section of the 12m channel in '*ab*' plane as viewed through the 12m windows in the perpendicular direction is shown. A typical minimum energy configuration of the molecule during the diffusion is also included.

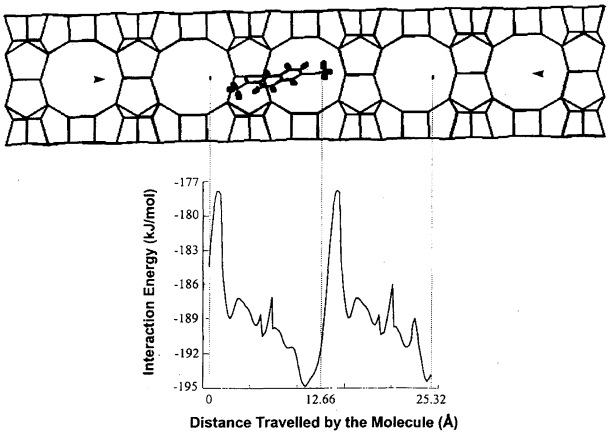

Fig. 9. Variation of interaction energy of **3** and the BEA framework as the molecule diffuses through the 12m channel. The cross section of the 12m channel in '*ab*' plane as viewed through the 12m windows in the perpendicular direction is shown. A typical minimum energy configuration of the molecule during the diffusion is also included.

energy values. Hence, the mean-energy values and the diffusivity given in Table 3 indicate that the diffusivity decreases in the order **3** > **1** > **4** > **2**. The diffusion energy barrier for **3** is much smaller than those of **2** and **4**. These results indicate that the pore dimensions, shape of the pores and their correspondence to the size and shape of the molecules determine the diffusion characteristics of the molecules. Overall,

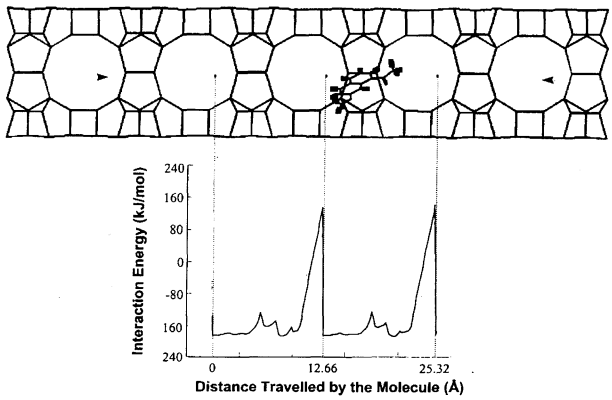

Fig. 10. Variation of interaction energy of **4** and the BEA framework as the molecule diffuses through the 12m channel. The cross section of the 12m channel in '*ab*' plane as viewed through the 12m windows in the perpendicular direction is shown. A typical minimum energy configuration of the molecule during the diffusion is also included.

these results indicate that there will be high selectivity for the diffusion of **3** in the case of BEA. The deformation of the molecules is always noted in the high-energy configuration during modeling. The amount of deformation can be correlated to the observed energy barriers, as shown in Table 4.

General Features: Modeling studies of the diffusion characteristics of acylated 2-methoxynaphthalene inside large-pore zeolites indicate that though the formation of 2-acyl-6-methoxynaphthalene is possible inside the pores of many large pore zeolites, the maximum selectivity will probably be achieved in BEA. The diffusivity of the molecules is controlled by the heterogeneity of the adsorption sites on the channel walls. The interaction energy of the molecules with the zeolite framework has been calculated for at least 100 locations along the diffusion path. The mean energy, which is a numerical mean of the interaction energy at all locations, was calculated and compared with the minimum energy to estimate the diffusivity. The diffusivity parameter is always in the range of 0 to 1, and values closer to 1 indicate higher diffusivity. The diffusion energy barrier (the difference between the highest energy configuration and the lowest energy configuration) is a useful parameter in addition to the diffusivity.

In addition to the diffusion of product molecules there are several other factors which control product formation in the reactions. These factors include the conformational flexibility of the molecules at different temperatures, the bulkiness of the intermediates formed, and the chemical composition of the zeolite framework. Thus, molecular-dynamic simu-

Table 4. Strain Energy (kJ mol^{-1}) of the Isomers of Acylated Products in Their Maximum and Minimum Energy Configurations in BEA

Molecule	Energy of the molecule at the peak maxima	Energy of the molecule at the deep minima
2	532.807	384.840
3	324.449	322.802
4	611.099	357.712

lations and electronic-structure calculations will be required to understand the finer aspects of product selectivity. In fact, one of the experimental studies[12] carried out at higher temperatures shows a product selectivity contrary to the predictions made in this study, which may be due to the influence of factors other than the diffusivity.

Conclusions

In this work, we demonstrate the efficiency of force field energy minimization techniques to study the adsorption and diffusion behavior of large molecules in the micropores of zeolites. The salient conclusions arising from the results of modeling studies and based on the above discussions are:

1) The diffusivity and diffusion energy barrier can be used to study the diffusion characteristics of molecules inside zeolites. The low energy barriers are necessary conditions for the diffusion of molecules, whereas, the diffusivity is qualitative sufficient condition.

2) The diffusion energy profiles are sensitive to size and shape of molecules as well as to the size and shape of zeolite pores.

3) The deformation of the molecules inside the constrained space of the zeolite pores is a major contributing factor for the high-energy configurations in addition to the zeolite – molecule interactions (Table 4).

4) These calculations show that a significant energy barrier difference exists for 2-acyl-6-methoxynaphthalene and other isomers in BEA and MOR. Thus, BEA and MOR could be expected to be shape-selective. In LTL, the diffusion energy barrier for the molecules increases in the order 1-acyl-7-methoxynaphthalene < 2-acyl-6-methoxynaphthalene < 1-acyl-2-methoxynaphthalene. Thus the order of selectivity in shape selective production of 2-acyl-6-methoxynaphthalene in these zeolites will be BEA > MOR > LTL.

References

1 C. G. M. Villa and S. P. Panossian, in "Chirality in Industry," ed by A. N. Collins, G. N. Sheldrake, and J. Crosby, John Wiley & Sons, New York (1992), p. 303.

2 J. A. Walker, D. R. White, and W. G. Salmond, U. S. Patent 4107439 (1978).

3 A. S. C. Chan, U. S. Patent 5233084 (1993).

4 G. E. Deckner, M. A. Rinaldi, and V. C. Szymanski, U. S. Patent 5824666 (1998).

5 D. L. Bissett, R. D. Bush, and R. Chatterjee, U. S. Patent Appl. 744891 (1998).

6 P. H. Gore, *Chem. Rev.*, **55**, 229 (1955).

7 P. H. Gore, in "Friedel-Crafts and Related Reactions," ed by G. A. Olah, Wiley Interscience, New York (1964), Vol. III, p. 72.

8 T. S. Cantrell, *J. Org. Chem.*, **32**, 1669 (1967).

9 E. A. Gunnewegh, R. S. Downing, and H. van Bekkum, *Stud. Surface Sci. Catal.*, **97**, 447 (1995).

10 L. Rand and R. J. Dolinski, *J. Org. Chem.*, **31**, 4061 (1996).

11 B. Chiche, A. Finiels, C. Gauthier, and P. Geneste, *J. Org. Chem.*, **51**, 2128 (1986).

12 G. Harvey and G. Mader, *Collect. Czech. Chem. Commun.*, **57**, 862 (1992).

13 A. Corma, M. J. Climent, H. Garcia, and J. Primo, *Appl. Catal.*, **49**, 109 (1989).

14 A. Finiels, A. Calmettes, P. Geneste, and P. Moreau, *Stud. Surface Sci. Catal.*, **78**, 595 (1993).

15 F. Richard, J. Drouillard, H. Carreyre, J. L. Lemberton, and G. Perot, *Stud. Surface Sci. Catal.*, **78**, 601 (1993).

16 A. Myata, K. Matsunaga, and M. Ishikawa, Japan Patent 07173096 (1995).

17 E. A. Gunnewegh, S. S. Gopie, and H. van Bekkum, *J. Mol. Catal.*, **A106**, 155 (1996).

18 B. M. Choudary, M. Sateesh, M. L. Kantam, and K. V. Ramprasad, *Appl. Catal.*, **171**, 155 (1998).

19 G. D. Yadav and M. S. Krishnan, *Stud. Surface Sci. Catal.*, **113**, 259 (1998).

20 P. J. Harrington and E. Lodjewijk, *Org. Proc. Res. Dev.*, **1**, 72 (1997).

21 J. A. Hyatt and P. W. Raynolds, *J. Org. Chem.*, **49**, 384 (1984).

22 J. A. Joeller and C. E. Sumner, *J. Org. Chem.*, **55**, 319 (1990).

23 A. T. Hagler, S. Lifson, and P. Dauber, *J. Am. Chem. Soc.*, **101**, 5122 (1979).

24 P. Dauber-Osguthorpe, V. A. Roberts, D. J. Osguthorpe, J. Wolff, M. Genest, and A. T. Hagler, *Proteins: Struct., Funct. Genet.*, **4**, 31 (1988).

25 R. C. Deka and R. Vetrivel, *J. Catal.*, **174**, 88 (1998).

26 A. Chatterjee and R. Vetrivel, *J. Chem. Soc., Faraday Trans.*, **91**, 4313 (1995).

27 A. Alberti, P. Davoli, and G. Vezzalini, *Z. Kristallogr.*, **175**, 249 (1986).

28 J. M. Newsam, *J. Phys. Chem.*, **93**, 7689 (1989).

29 J. M. Newsam, M. M. J. Treacy, W. T. Koesteir, and C. B. De Gruyter, *Proc. R. Soc. London*, **A420**, 375 (1988).

30 J. A. Horsley, J. D. Fellmann, E. G. Derouane, and C. M. Freeman, *J. Catal.*, **147**, 231 (1994).

31 R. Vetrivel, C. R. A. Catlow, and E. A. Colbourn, *Stud. Surface Sci. Catal.*, **49**, 795 (1989).

32 Y. Nakazaki, N. Goto, and T. Inui, *J. Catal.*, **136**, 142 (1992).

33 R. Millini and S. Rossini, *Stud. Surface Sci. Catal.*, **105**, 1389 (1996).

34 R. C. Deka and R. Vetrivel, *Chem. Commun.*, **1996**, 2397.

35 P. Bharathi, R. C. Deka, S. Sivasanker, and R. Vetrivel, *Catal. Lett.*, **55**, 113 (1998).